Laser and Particle Beams (2008), *26*, 649–660. Printed in the USA.

doi:10.1017/S0263034608000700

Inverse Compton backscattering source driven by the multi-10 TW laser installed at Daresbury

G. PRIEBE,[1] D. LAUNDY,[1] M.A. MACDONALD,[1] G.P. DIAKUN,[1] S.P. JAMISON,[3] L.B. JONES,[1,3] D.J. HOLDER,[1,3] S.L. SMITH,[1,3] P.J. PHILLIPS,[4] B.D. FELL,[1] B. SHEEHY,[8] N. NAUMOVA,[9] I.V. SOKOLOV,[11] S. TER-AVETISYAN,[10] K. SPOHR,[12] G.A. KRAFFT,[13] J.B. ROSENZWEIG,[14] U. SCHRAMM,[6] F. GRÜNER,[7] G.J. HIRST,[5] J. COLLIER,[5] S. CHATTOPADHYAY,[2] AND E.A. SEDDON[1]

[1]Science and Technology Facilities Council, Daresbury Laboratory, Cheshire, United Kingdom
[2]Cockcroft Institute, Daresbury Science and Innovation Campus, Warrington, United Kingdom
[3]Accelerator Science and Technology Centre, Daresbury Laboratory, Cheshire, United Kingdom
[4]University of Dundee, Division of Electronic Engineering and Physics, Dundee, United Kingdom
[5]STFC Rutherford Appleton Laboratory, Chilton, Didcot, United Kingdom
[6]Forschungszentrum Dresden-Rossendorf, Dresden, Germany
[7]Max-Planck-Institut für Quantenoptik, Garching, Germany
[8]Sheehy Scientific Consulting, Wading River, New York
[9]Laboratoire d'Optique Appliquee, Chemin de la Huniere, Palaiseau, France
[10]School of Mathematics and Physics, Queen's University Belfast, Belfast, United Kingdom
[11]Space Physics Research Laboratory, University of Michigan, Ann Arbor, Michigan
[12]Department of Electronic Engineering and Physics, University of Paisley, Glasgow, United Kingdom
[13]Thomas Jefferson National Accelerator Facility, Jefferson Avenue, Newport News, Virginia
[14]University of California at Los Angeles, Department of Physics and Astronomy, Los Angeles, California

(Received 1 May 2008; Accepted 3 August 2008)

Abstract

Inverse Compton scattering is a promising method to implement a high brightness, ultra-short, energy tunable X-ray source at accelerator facilities. We have developed an inverse Compton backscattering X-ray source driven by the multi-10 TW laser installed at Daresbury. Hard X-rays, with spectral peaks ranging from 15 to 30 keV, depending on the scattering geometry, will be generated through the interaction of laser pulses with electron bunches delivered by the energy recovery linac machine, initially known as energy recovery linac prototype and subsequently renamed accelerators and lasers in combined experiments. X-ray pulses containing 9×10^7 photons per pulse will be created from head-on collisions, with a pulse duration comparable to the incoming electron bunch length. For transverse collisions 8×10^6 photons per pulse will be generated, where the laser pulse transit time defines the X-ray pulse duration. The peak spectral brightness is predicted to be $\sim 10^{21}$ photons/(s mm^2 mrad^2 0.1% $\Delta\lambda/\lambda$).

Keywords: ALICE; Compton scattering; Compton synchrotron radiation; Energy recovery linac; ERLP; Laser Compton scattering; Laser synchrotron radiation; Thomson scattering; Ultra-short X-ray pulses; X-ray source

INTRODUCTION

Knowledge of the atomic structure of matter is of fundamental importance in science. The discovery of structural information has often led to the creation of new scientific fields. Advances in solid state physics followed the discovery of crystal structures obtained through the production of X-ray diffraction patterns (von Laue, 1936). The modern science of molecular biology and genetic engineering were triggered by the discovery of the double helix structure of DNA (Watson & Crick, 1953). X-ray diffraction gives precise information about atomic structure on a sub-angstrom scale and spectroscopic techniques—extended X-ray absorption fine structure (EXAFS), X-ray absorption near edge structure (XANES)—give information about local order and on chemical states. The possibility of generating ultra-short X-ray pulses provides an opportunity to capture structural

Address correspondence and reprint requests to: G. Priebe, STFC, Daresbury Laboratory, Daresbury, Warrington, Cheshire, WA4 4AD, UK. E-mail: gerd.priebe@stfc.ac.uk

and electronic changes dynamically, for example, observing the detailed intermediate steps of chemical reactions with atomic resolution. Typical time scales for changes in atomic configurations are comparable with the cyclic duration of molecular vibrations. Advances in the generation of ultra-short laser pulses over the past two decades have made it possible to observe these fundamental processes. These advances have taken science from the ns- and ps-regime a generation ago, to the fs time scale in the past decade, and recently into the as-regime (Strickland & Mourou, 1985; Sansone *et al.*, 2006; Baker *et al.*, 2006; Baeva *et al.*, 2007). The fact that the wavelength of these ultra-short laser light sources is significantly larger than the sizes and distances of the constituent atoms in the molecules, and crystals under study has meant that information on structural changes could only be inferred from observation of the secondary effects that these structural changes have on optical properties.

The recent development of small, affordable, high-power lasers based on chirped pulse amplification (CPA), capable of producing fs pulses has produced interesting opportunities into the development of table-top size X-ray sources. Several ns and ps X-ray techniques based on both synchrotron and table-top X-ray sources have been developed during the past decade (Helliwell & Rentzepis, 1997). Most of these techniques use an ultra-short laser pulse to initiate a photo reaction in the sample that is then studied by a delayed ultra-short X-ray pulse, which probes the structural changes that take place in the sample. In the solid state, non-thermal melting and laser-induced heat and strain propagation in metal and semiconductor single and mosaic-crystals have been studied by means of time-resolved X-ray diffraction with ns to ps time resolution (Tomov *et al.*, 1999; Siders *et al.*, 1999). The use of all of these techniques in conjunction with a fs X-ray source will allow the direct measurement of structural information in many ultra-fast fundamental physical, chemical and biological processes, currently inaccessible with the time resolution of existing sources.

The development of short and ultra-short X-ray sources will drive many important scientific applications by enabling direct measurement of atomic motion and structural changes in the condensed phase. Perhaps the most important feature of these new sources of ultra-short X-ray pulses is that they enable physical experiments combining fs time resolution and atomic scale spatial resolution.

There are several different ways to generate short and ultra-short X-ray pulses (Kim *et al.*, 1994; Materlik *et al.*, 1995; Schoenlein *et al.*, 1996, 2000*a*, 2000*b*; Leemans *et al.*, 2000; Catravas *et al.*, 2001; Guo *et al.*, 2001; Service, 2002; Hafz *et al.*, 2003; Phuoc *et al.*, 2003; Umstadter, 2003; Xia *et al.*, 2004; Janulewicz *et al.*, 2004*a*, 2004*b*, 2005; Krafft, 2004, 2005; Lucianetti *et al.*, 2004; Giulietti *et al.*, 2005; Tümmler *et al.*, 2005; Zhavoronkov *et al.*, 2005; Riley *et al.*, 2005; Legall *et al.*, 2006; Notley *et al.*, 2006; Khattak *et al.*, 2007; Chen *et al.*, 2008; Abdallah *et al.*, 2007; Mangles *et al.*, 2006) such as ultra-short laser-generated K_α sources, X-ray free-electron lasers, electron bunch-slicing in synchrotrons, and the one to be discussed here, inverse Compton scattering of an intense laser pulse from a high-brightness electron beam.

Using the laser effectively as an undulator, which confers a much shorter period than the commonly used magnetic undulators in synchrotron light sources, means a lower energy electron beam can be used to deliver X-rays. This source also offers a wide tuning range, where X-ray source parameters such as photon energy, brightness, bandwidth, and pulse length can be tuned through the laser and electron beam parameters as well as the interaction geometry of the beams. The interaction can also be viewed as a collision between an electron and photon. This treatment of the system gives rise to Compton scattering, or Thomson scattering when the incident photon energy in the electron rest frame is much less than mc^2. Depending on the reference frame, it can appear as though the electrons have been energized by the photons or, if the electrons are moving relativistically, the energy is instead transferred from electrons to photons, therefore the opposite of Compton scattering—inverse Compton scattering—occurs. The frequency of the photons scattered from the relativistic electron beam is dependent on the interaction angle of the two beams, this typically range from 90° to 180°, although small-angle Thomson scattering has also been a proposed interaction configuration (Huang *et al.*, 1994). The generation of 300 fs hard X-ray pulses has been demonstrated using 90° Thomson scattering between fs laser pulses and tightly-focused ns electron bunches in a synchrotron (Kim *et al.*, 1994). The relatively low X-ray flux of $\approx 10^6$ photons/s obtained in these experiments could be significantly increased by the use of higher laser powers and the use of high quality fs electron bunches.

However, the most promising feature of laser based X-ray sources in time resolved studies, is the intrinsic synchronisation of a laser induced change in a material with the probing X-ray probe pulse. As already demonstrated a photon flux of 10^6 photon per second (Li *et al.*, 2005) on the sample can be sufficient for time resolved X-ray spectroscopy. Additional improvement of the experimental condition can perhaps be achieved by using more efficient X-ray optics for spectral measurements (Legall *et al.*, 2006).

In this paper, we describe a new source of ultra-short X-ray pulses based on inverse Compton scattering of multi-10 TW, 100 fs laser-pulses with 35 MeV electron bunches delivered by the energy recovery linac prototype (ERLP) recently renamed to accelerators and lasers in combined experiments (ALICE), which is being commissioned by the Daresbury Laboratory (Fig. 1; Smith *et al.*, 2005).

Thomson scattering from a relativistic electron beam has been extensively studied theoretically both in the linear and the nonlinear regime. For clarity, we adapt the linear theory, where the energy of the scattered photon is calculated using energy and momentum conservation, and the differential scattering cross-section is calculated using quantum

https://doi.org/10.1017/S0263034608000700 Published online by Cambridge University Press

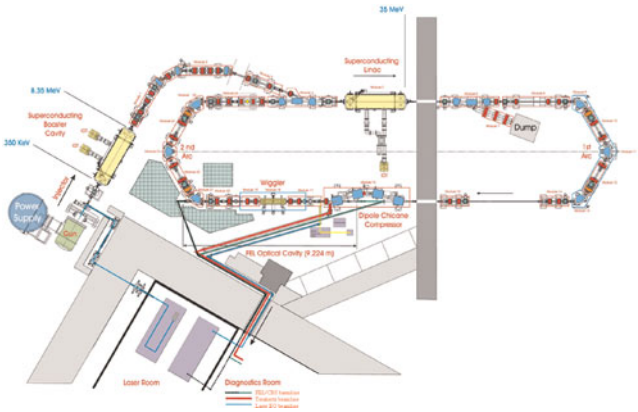

Fig. 1. (Color online) Layout of the energy recovery linac machine ALICE commissioned at Daresbury Laboratory.

electrodynamics theory. The X-ray source, the inverse compton backscattering X-ray source driven by the table-top 10 TW (T^3-laser) laser installed at Daresbury (COBALD) will initially be used as a short pulse diagnostic for the ERLP electron beam (Leemans *et al.*, 1996, 1997; Ross *et al.*, 1997; Tannebaum & Shintake, 1999; Hartemann *et al.*, 2004; Chouffani *et al.*, 2006). It will explore the extreme challenges of photon/electron-beam synchronization, which are a fundamental requirement for the next generation of accelerator-based light sources. The COBALD source will be exploited for a fast melting experiment (Wark, 1999; Sundaram & Mazur, 2002; von der Linde, 2003; Sokolowski-Tinten & von der Linde, 2004) providing information about the synchronization between the laser pulse and the electron bunch, and on X-ray source stability. In the experiment, a portion of the laser beam will be used to induce disorder at the surface of a crystal, which will subsequently recrystallizes on a ps time scale. The X-ray pulse will probe the recrystallization by allowing the measurement of the diffracted X-ray intensity from the crystal lattice at intervals throughout the transformation. The inverse Compton backscattering (CBS) source has the high-brightness, short pulses, and tunable energy and represents a research tool, capable of measuring on an atomic scale with high spatial and temporal.

Energy Recovery Linac

Synchrotron radiation (SR) X-ray sources have come a long way from their first parasitic existence on high energy physics machines. Improvements in electron storage rings and insertion devices have led to an exponential increase in brilliance for each successive generation of sources. The technology of storage rings has reached maturity, resulting in third generation SR facilities that are capable of providing beam qualities close to the physical limits(Ozaki *et al.*, 2006). The fundamental X-ray beam properties of ring sources, such as the source size, brilliance, and pulse duration are limited by the equilibrium between the electron beam and the magnet lattice. In contrast to storage rings, linear accelerators can produce both low emittance and very short bunches, because the limitations set by this equilibrium are not an issue. As a result, several proposed large light-source projects are based on linear accelerators. However, in a traditional linear accelerator, the absence of beam recirculation would lead to an enormous power consumption if high average currents are to be obtained. To circumvent this prohibitively large power consumption, energy recovery linac (ERL) technology (Tigner, 1965) is being explored for next-generation synchrotron light sources; in such accelerators the energy delivered to the electron beam is re-circulated, rather than the electron beam itself.

The use of ERLs enables electron beams with extraordinary brilliance, with small source size, ultra-short pulses, and concomitant high transverse coherence. Several laboratories have proposed high-power ERLs for the production of high-brightness radiation. Accelerators for different parameter sets and various applications are being worked on by Cornell University, Argonne National Laboratory, Budker Institute, High Energy Accelerator Research Organization (KEK), and Jefferson Laboratory (Kulipanov *et al.*, 1998; Bazerov *et al.*, 2001; Suwada *et al.*, 1997; Smith *et al.*, 2007; Neil *et al.*, 2005; Borland, 2006). ALICE, at Daresbury Laboratory (Fig. 1, Table 1), is also an advanced energy recovery linac based light source (Poole *et al.*, 2003; Smith *et al.*, 2005).

It is based on a combination of a direct current photocathode electron gun, a superconducting injector linac, and main linac operating in energy recovery mode. A infrared free electron laser cavity (IR-FEL) is incorporated in the machine. The FEL is based on a permanent magnet array undulator that will deliver intense short pulses of photons in the wavelength range 4 μm to 12 μm. The 1.4 ps pulses will deliver ~3×10^{14} photons per pulse, with a pulse energy of 13.3 μJ. The priorities for this machine are to gain experience with operating a photo-injector gun and superconducting linac; to produce and maintain high-brightness electron beams; to achieve energy recovery from a FEL-cavity disrupted beam and to study important synchronization issues, all of which will contribute towards the design of a larger scale fourth generation light source.

Table 1. *The main parameters of the energy recovery linac machine ALICE*

	ALICE
Gun energy	350 keV
Max energy	35 MeV
Charge/Bunch	80 pC
Bunch rep. rate	81.25 MHz
Post chicane bunch length	350 fs
Focused beam size	X ≈ 20 μm
	Y ≈ 50 μm
Energy spread	0.2%
Normalized emittance	5 mm mrad

https://doi.org/10.1017/S0263034608000700 Published online by Cambridge University Press

Multi-10 TW Laser

The customized table-top CPA multi-10 TW laser system (COHERENT)—installed at the high field laser facility at Daresbury—contains an ultra-short, bandwidth-limited, Kerr-lens mode-locked (Spence *et al.*, 1991; Brabec *et al.*, 1992; Stingl *et al.*, 1995). Ti:sapphire master oscillator (Micra; $\Delta\lambda > 100$ nm) with a repetition rate of 81.25 MHz, followed by a stretcher and a regenerative amplifier (2.8 mJ @ 1 kHz), which is used as a front-end system (Fig. 2) for a four-pass Ti:Sa power amplifier.

The output of the master oscillator exhibits a broad spectrum centered at 800 nm. The pulses are then passed through a one-to-one imaging, single grating stretcher to obtain a pulse-width of about 150 ps before they are injected as seed into the regenerative amplifier (legend), which is pumped by a diode-pumped, intra-cavity doubled, Q-switched Nd:YLF laser (evolution). The customized power amplifier, which contains a large aperture Ti:Sa crystal (Fig. 3, left), pumped from both ends (relay imaged) using two spatially optimized frequency doubled Nd:YAG lasers operating at 10 Hz, amplifies the pulses up to 1.5 J in a bow-tie configuration before recompression (Fig. 3, right).

For further applications as laser-driven plasma sources and particle acceleration, a pulse cleaner (Divall & Ross, 2004; Priebe, 2006) using a fast pockels-cell driven by a KENTECH fast pulse generator will be established. The legend incorporates an additional compressor to use the recompressed pulses (2.2 mJ @ 1 kHz) for further applications. Figure 4 shows the layout of the laser beam lines for further applications.

One of the applications of the kHz beam will be the development of non-destructive longitudinal, i.e., temporal, diagnostics of the accelerator electron bunches; the Coulomb field of an electron bunch interacts, through the electro-optic (EO) effect, with a probe laser pulse in an in vacuo non-linear crystal. The temporal evolution of the Coulomb field is encoded as a time-dependent probe polarization (EO-sensing) (Berden *et al.*, 2004; Jamison *et al.*, 2006). The kHz beam also drives a stand-alone THz-source, with the terahertz-radiation produced by either optical rectification or a large area photo-conductive antenna; this THz-source provides radiation pulses that can mimic the relativistic Coulomb field, and hence allow significantly simplified testing of diagnostic concepts (Jamison *et al.*, 2003). The detailed laser parameters—measured during the installation at Daresbury—of the multi-10 TW laser system are given in Table 2.

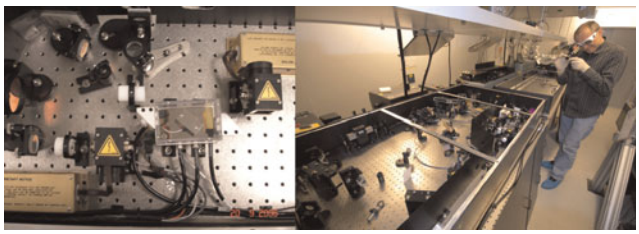

Fig. 2. (Color online) Installation of the regenerative amplifier front end including pulse-picker and kHz compressor.

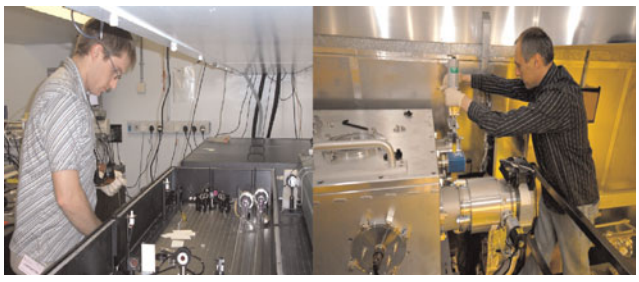

Fig. 3. (Color online) Installation of the multi-pass power amplifier (left) and the chirped pulse compressor (right).

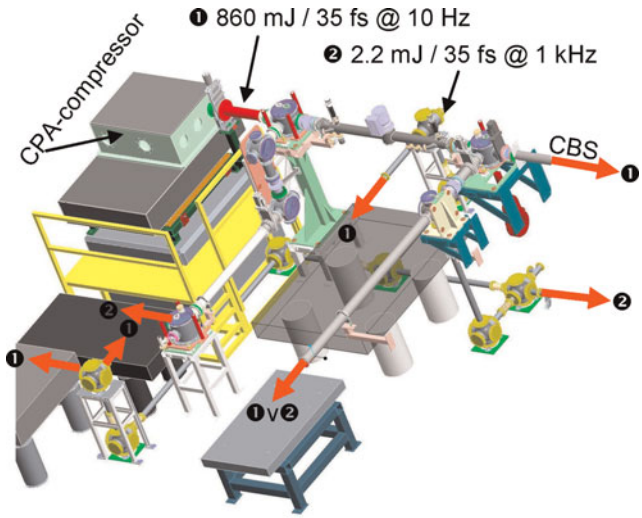

Fig. 4. (Color online) Laser beam lines from the laser front-end system (2.2 mJ @ 1 kHz) and from 4-pass Ti:Sa power amplifier through the CPA compressor to several application stations.

Table 2. *The main laser parameters of the customized (COHERENT) table-top multi-10 TW laser system installed at the Daresbury high field laser laboratory*

	kHz-Laser	TW-Laser
Wavelength	798 nm	802 nm
Bandwidth	30 nm	13 nm
Energy before compression	2.8 mJ	1500 mJ
Energy after compression	2.2 mJ	860 mJ
Pulse width	35 fs	98 fs/35 fs
Strahl ratio		0.6–0.8
M^2	1.2 *x*; 1.11 *y*	1.38 *x*; 1.45 *y*

INVERSE COMPTON SCATTERING

The discovery of the Compton effect (Compton, 1923) was a milestone in physics in which the quantum nature of light

https://doi.org/10.1017/S0263034608000700 Published online by Cambridge University Press

was finally proved. The Compton effect is the inelastic scattering of X-rays by electrons. The electrons gain energy in the process and the Compton scattered X-rays are observed at lower energy than the incident X-rays. Due to the kinematics of the scattering process, there is a fixed relationship between the energy of the scattered X-rays and the angle through which they are scattered. Soon after the discovery of the Compton effect, it was realized that electron motion during the scattering process Doppler-broadens the emission spectrum—at fixed scattering angle—and it is this Doppler shift that forms the basis of inverse Compton X-ray sources. In inverse Compton scattering, the electrons are highly energetic, and the Doppler shift results in the scattered photons gaining significant energy from the electrons. This process allows low energy photons, e.g., from an intense laser, when scattered by ultra relativistic electrons in an accelerator, to generate hard X-rays. If the energy of the incident photon $E_{\rm ph}$ in the frame of the interaction is much less than $m_{\rm e}c^2$, the Thomson scattering cross-section ($\sigma_{\rm Th} = (8\pi/3)r_{\rm e}^2$) can be used to describe the probability of scattering, where $m_{\rm e}$ is the rest mass of the electron, and $r_{\rm e}$ is the classical electron radius. In the laboratory frame, the scattered laser photons are relativistically up-shifted in frequency into the hard X-ray range and are emitted into a narrow cone. Alternatively, the interaction can be viewed in the electron rest mass frame, the incident laser pulse then appears as an electromagnetic undulator of wavelength $\lambda_{\rm u} = \lambda_{\rm ph}/\gamma(1-\beta\cos\Phi)$, where γ is the relativistic factor $E_{\rm e}/m_{\rm e}c^2$, β is the velocity of the electrons relative to the speed of light, and Φ is the angle of incidence between electron and laser beams. The undulating electrons radiate photons, which are frequency up-shifted, in the laboratory frame, by a second factor of 2γ. In the laboratory frame, the X-rays are confined to a narrow cone with opening angle about $1/\gamma$ in the electron beam propagation direction. The X-ray energy E_γ varies with the observation angle θ in the laboratory frame due to the kinematics of the scattering

$$E_\gamma = \frac{2\gamma^2(1-\beta\cos\Phi)}{1+(a_0^2/2)+\gamma^2\theta^2}E_{\rm ph},$$

where $a_0 = eE_{\rm ph}\lambda_{\rm ph}/2\pi m_{\rm e}c^2$ is the normalized vector potential of the laser field, analogous to the undulator deflection parameter $K = eB_0\lambda_{\rm u}/2\pi m_{\rm e}c^2$ of a static field undulator (Brown & Kibble, 1964; Sarachik & Schappert, 1970; Alferov *et al.*, 1974; Coisson, 1979; Kim, 1989). The peak X-ray energy for transverse interaction ($\Phi = \pi/2$) is half that for head-on collisions ($\Phi = \pi$). Due to the similarity between synchrotron radiation and inverse Compton scattering, the radiation is often called laser synchrotron radiation or Compton synchrotron radiation. Using this analogy, and replacing the magnetic undulator with a laser beam of 10^4 times smaller period, the electrons are deflected many more times and contribute to coherent energy gain with electron beams 100 times less energetic than in a conventional magnetic undulator. When $a_0 \ll 1$, the interaction is in the linear regime; when $a_0 \geq 1$ the interaction is in the nonlinear regime with higher order harmonics, which may be used to extend the tuning range of the X-ray source (Ride *et al.*, 1995; Salamin & Faisal, 1996). However, ponderomotive scattering (Krafft, 2004, 2005) also starts to occur for $a_0 > 1$, where the electrons are deflected from the laser focus point before they are able to scatter the photons, therefore decreasing the total flux of emitted X-rays (Chen *et al.*, 2008). The precise intensity and spectral profile of the resultant X-ray beam is closely linked to the laser frequency and bandwidth, the electron beam emittance, energy and energy spread, and the interaction and focusing geometries (Hartemann *et al.*, 2001). A schematic illustration of the inverse Compton scattering geometry is shown in Figure 5.

From the particles point of view, the photon strikes an electron of energy $E_{\rm e}$- with an angle of incidence Φ. In the electron's rest frame, the energy of the photon is Doppler up-shifted to $E_{\rm ph'} = \gamma(1+\cos\Phi)E_{\rm ph}$ and the wavelength of the scattered photon is given by the Compton formula $\lambda_\gamma - \lambda_{\rm ph'} = \lambda_{\rm c}(1-\cos\theta')$, where $\lambda_{\rm c} = h/m_{\rm e}c$ is the Compton wavelength, h is the Planck's constant, and θ' is the scattering angle in the electron rest frame. The scattered photons gain energy $E_{\gamma'} = m_{\rm e}c^2E_{\rm ph'}/[m_{\rm e}c^2 + (1-\cos\theta')E_{\rm ph'}]$, with the contracted angle $\cos\theta' = (\cos\theta-\beta)/(1-\beta\cos\theta)$ satisfying the momentum conservation constraint. Since the relativistic Doppler up-shifted X-ray energy $E_{\rm ph'}$ is much less that $m_{\rm e}c^2$ in the electron rest frame, the center of momentum frame is very close to that of the relativistic electron. Using the back transformation in the laboratory frame $E_\gamma = \gamma(1-\beta\cos\theta)E_{\gamma'}$ results in the relation between the scattered photon energy E_γ and that of the incident laser photon energy $E_{\rm ph}$ and electron energy $E_{\rm e}$- being given by: $E_\gamma = E_{\rm ph}(1-\beta\cos\Phi)/[(1-\beta\cos\theta) + E_{\rm ph}(1-\beta\cos\theta-\Phi)/E_{\rm e}$-]. The dependence of the energy of the scattered X-ray photons on the collison angle Φ between the laser photons and the electrons, and on the scattering angle θ, is shown in Figure 6, for the laser and electron parameters at Daresbury (Tables 1 and 2).

For a fixed laser incidence angle, there is a unique relation between the resultant scattered energy E_γ and the photon

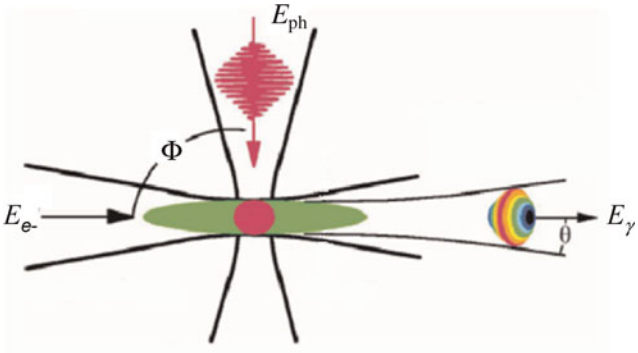

Fig. 5. (Color online) Interaction geometry of inverse Compton scattering.

https://doi.org/10.1017/S0263034608000700 Published online by Cambridge University Press

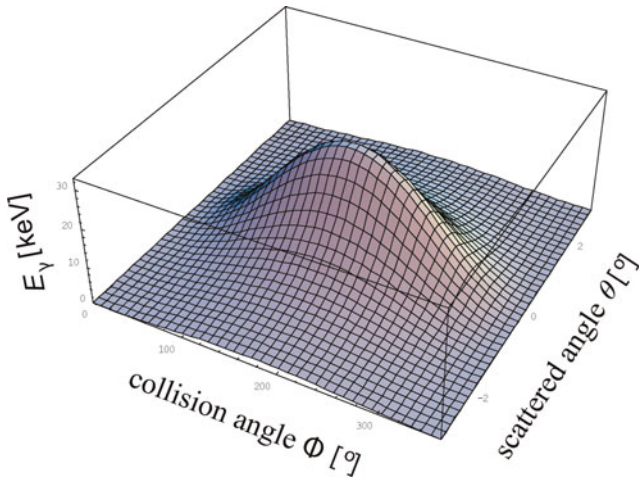

Fig. 6. (Color online) Dependence of the X-ray energy E_γ on the interaction geometry—the collision angle Φ—and the scattering angle θ.

trajectory of the X-rays. The peak X-ray energy ($\theta = 0$) for head-on collisions ($\Phi = \pi$) and transverse interaction ($\Phi = \pi/2$) simplifies—using $E_{\mathrm{ph}} \ll m_e c^2$, $\beta \approx 1$, and $\gamma = (1-\beta^2)^{-1/2}$—to the expected result:

$$\text{head-on collision:} \quad E_\gamma\big|^{\theta=0}_{\Phi=\pi} \approx 4\gamma^2 E_{\mathrm{ph}} \approx 30\,\mathrm{keV}$$

$$\text{transverse collision:} \quad E_\gamma\big|^{\theta=0}_{\Phi=\pi/2} \approx 2\gamma^2 E_{\mathrm{ph}} \approx 15\,\mathrm{keV}.$$

In practice, the X-ray spectrum is broadened by the bandwidth, and the divergence of the laser pulse as well as the energy spread and the divergence of the electron bunch (Table 3). The energy spread depends linearly on the laser energy spread and quadratically on the electron energy spread. The energy spread of the bandwidth-limited laser pulse is given by $\Delta E_{\mathrm{ph}} = ch\Delta\lambda/\lambda^2$, where $\Delta\lambda$ is given by the time-bandwidth product $\tau_{\mathrm{ph}} c\Delta\lambda/\lambda^2 = 2\ln 2/\pi$ if the pulse shape is Gaussian and where τ_{ph} is the laser pulse duration. For a 100 fs laser pulse the energy spread is therefore $\Delta E_{\mathrm{ph}}/E_{\mathrm{ph}} \approx 1.2\%$ and $\Delta E_{\mathrm{ph}}/E_{\mathrm{ph}} \approx 3.9\%$ for a 30 fs laser pulse.

Using an off-axis parabolic mirror with a focal length f of 1780 mm for head-on interaction and 1230 mm for transverse interaction, to focus the laser beam gives a focused spot size ($2\lambda f/\pi\varnothing$) of ≈40 μm with an opening angle of ≈1.4° and a focal length (twice the Raleigh length $z_R = \pi w_0 2/\lambda$) of ≈3 mm for head-on collision, and a spot size of ≈28 μm with an opening angle of ≈2.1° and a focal length of ≈1.5 mm for transverse collision.

Table 3. *X-ray energy broadening induced by the wavelength bandwidth and the divergence of the laser pulse as well as the energy spread and the divergence of the electron bunch*

		$\Delta E_\gamma/E_\gamma$ [%]
Laser pulse	Wavelength bandwidth	1.2
	Divergence [$\Phi = \pi$ | $\Phi = \pi/2$]	0.004 | 1.8
Electron bunch	Energy spread	0.4
	Divergence [$\Phi = \pi$ | $\Phi = \pi/2$]	0.0003 | 0.4

The divergence of the electron bunch is ≈0.2° given by the normalized emittance and the spot size σ_e of the electron focus ($\Delta\theta_e = \varepsilon_n/\gamma\beta\sigma_e$). In head-on collision, the on-axis X-ray energy spread caused by the divergence of the photons, and of the electrons is negligible (0.004% | 0.0003%) compared with the broadening due to their own energy spread (Fig. 7). For transverse interaction, the divergence of the photons becomes the dominating factor (1.8%) and the energy spread induced by the divergence of the electrons (0.4%) becomes comparable to the energy spread itself.

In the rest frame of the electron bunch, the differential scattering cross-section is described by the Klein–Nishina formula (Klein & Nishina, 1929):

$$\frac{d\sigma_c}{\sin\theta' d\theta'} = \pi r_e^2\, \varepsilon'^2 \left[\varepsilon' + \frac{1}{\varepsilon'} - 1 + (\cos\theta')^2\right],$$

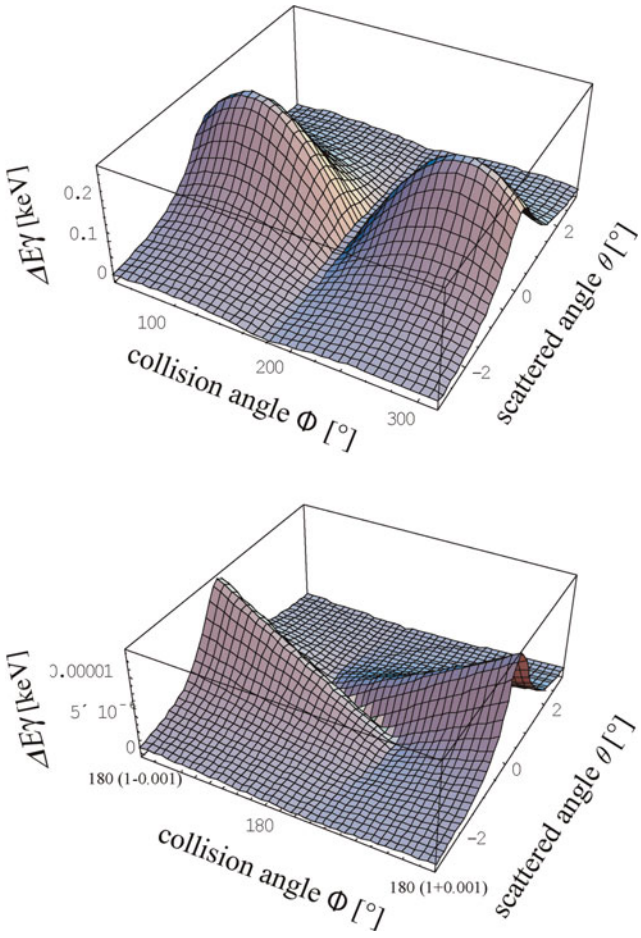

Fig. 7. (Color online) X-ray energy spread ΔE_γ due to the divergence of the laser beam (top) and the detailed distribution of the X-ray energy spread ΔE_γ for head-on collision geometry (bottom) as a function of the collision angle Φ and the scattering angle θ.

https://doi.org/10.1017/S0263034608000700 Published online by Cambridge University Press

where ε' is the ratio between the energies of the scattered and incident photon $\varepsilon' = E_{\gamma'}/E_{\mathrm{ph}'}$. If the interaction is such that the recoil momentum of the electron can be disregarded, $E_{\mathrm{ph}} \ll m_e c^2$ ($\varepsilon' = 1$), then this leads to the well known $(\cos\,\theta)^2$ distribution of dipole radiation and the differential Thomson scattering cross-section:

$$\frac{d\sigma_{\mathrm{Th}}}{d\theta'} = \pi r_e^2 [1 + (\cos\,\theta)^2]$$

and integrated, gives the Thomson cross-section $\sigma_{\mathrm{Th}} = (8/3)\pi r_e^2 = 0.665 \times 10^{-28}\,\mathrm{m}^2$ for elastic scattering of a photon from an electron. The total cross-section for the non-relativistic $\varepsilon' \gg 1$ and the extremely relativistic $\varepsilon' \ll 1$ cases are given as:

$$\sigma \approx \sigma_{\mathrm{Th}}\left(1 - 2\varepsilon' + \frac{26\,\varepsilon'^2}{5} + \cdots\right), \quad \text{for} \quad \varepsilon' \gg 1,$$

$$\sigma \approx \frac{3}{8}\,\sigma_{\mathrm{Th}}\,\frac{1}{\varepsilon'}\left(\ln 2\varepsilon' + \frac{1}{2}\right), \quad \text{for} \quad \varepsilon' \ll 1.$$

Transforming the differential Klein–Nishina cross-section to the laboratory frame of reference, using the above mentioned boundary condition, as well as its derivative ($d\theta' \sin\,\theta' = d\theta\,\sin\,\theta(1-\beta^2)/(1-\beta\cos\,\theta)^2$) and the transformations $E_{\gamma'} \rightarrow E_\gamma$ and $E_{\mathrm{ph}'} \rightarrow E_{\mathrm{ph}}$ gives the differential Compton cross-section:

$$\frac{d\sigma_c}{\sin\,\theta\,d\theta} = \pi\,r_e^2\,\varepsilon^2\left[\varepsilon + \frac{1}{\varepsilon} - 1 + \left(\frac{\cos\,\theta - \beta}{1 - \beta\cos\,\theta}\right)^2\right],$$

with $\varepsilon = m_e c^2/[m_e c^2 + \gamma\,(1 + \cos\,\Phi)(1-(\cos\,\theta-\beta)/(1-\beta\,\cos\,\theta))E_{\mathrm{ph}}]$. The cross-section for scattering a photon into a cone of angle θ_c in the laboratory frame is then $\sigma_c(\theta_c) = \int d\theta(d\sigma_c/d\theta)$ and the average energy of X-rays backscattered in the laboratory frame is $(\int d\theta\,E_\gamma\,d\sigma_c/d\theta)/(\int d\theta\,d\sigma_c/d\theta)$. Limiting the integration to the opening half-angle of $1/2\gamma$ leads to a scattering cross-section independent of the electron energy. Numerically, this is 0.165 barn and of course integrating over the full phase space gives the Thomson cross-section of 0.665 barn.

The total number of X-ray photons N_γ scattered per unit time and volume into a cone of angle θ_c is given by the product of the electron beam four-current $j_\mu(x_\nu) = ecn_e(x_\nu)u_\mu/\gamma$ and the incident photon four-flux $\Phi_\mu(x_\nu) = cn_\lambda(x_\nu)k_\mu/\omega$ as $d^4N_\gamma(x_\nu)/d^4x_\nu = (\sigma_c/ec)j_\mu(x_\nu)\Phi_\mu(x_\nu) = (c\sigma_c/\gamma\omega)n_e(x_\nu)n_{\mathrm{ph}}(x_\nu)u_\mu k^\mu$ (Landau & Lifshitz, 1975). Here, $u_\mu = dx_\nu c\,dt$ is the electron four-velocity, $k^\mu = (\omega/c,\ k)$ is the incident photon four-wave number. The number of X-ray photons per unit time can be expressed in Cartesian coordinates explicitly as $d^4N_\gamma(x,y,z,t)/dx\,dy\,dz\,c\,dt = \sigma_c n_e(x,y,z,t)n_{\mathrm{ph}}(x,y,z,t)(1-\beta\,\cos\,\Phi)$ (Hartemann *et al.*, 2005):

$$N_\gamma = (1 - \beta\cos\,\Phi)\sigma_c\,L,$$

where $L = \int n_e n_{\mathrm{ph}}\,dx\,dy\,dz\,c\,dt$ is the luminosity, which is determined by the collision geometry of the electron bunch and the laser pulses. In order to evaluate the pulse length of the X-rays, we assume that both the electron bunch and the laser pulse satisfy the Gaussian distribution. The density profile of the laser light pulse and the electron bunch are thus given by:

$$n_{\mathrm{ph}} = \frac{N_{\mathrm{ph}}}{2\sqrt{2}\,c\pi^{3/2}}\frac{1}{w_{\mathrm{phx}}[z]w_{\mathrm{phy}}[z]\,\tau_{\mathrm{ph}}} \times \exp\left[-\frac{2x^2}{w_{\mathrm{phx}}^2[z]} - \frac{2y^2}{w_{\mathrm{phy}}^2[z]} - \frac{2(t-(z/c))^2}{\tau_{\mathrm{ph}}^2}\right]$$

$$n_e = \frac{N_e}{2\sqrt{2}\,c\pi^{3/2}}\frac{1}{w_{ex}w_{ey}w_{ez}} \times \exp\left[-\frac{x^2}{2w_{ex}^2} - \frac{y^2}{2w_{ey}^2} - \frac{(t+(z/\beta\,c))^2}{2w_{ez}^2}\right].$$

$w_{\mathrm{ph}x,y} = (w_0^2(1 + (z/z_r)^2))^{1/2}$ is the beam waist, N_{ph} is the total number of photons in the laser pulse, τ_{ph} is the pulse duration—which is related to the bandwidth as $\Delta\tau_{\mathrm{ph}}\,\Delta\omega = \sqrt{2}$, in the case of a Fourier-transform-limited pulse—w_0 is the $1/e^2$ focal radius, N_e is the total number of electrons in one bunch, $w_{ex,y}$ are the magnitude of the electron bunch in the x and y directions, and cw_{ez} is the bunch length. For laser pulses crossing the electron bunch at an angle Φ, the luminosity can be described as: $L = N_e N_{\mathrm{ph}}/[2\pi(w_{ey}^2 + w_{oy}^2/4)^{1/2}(\cos^2\,\Phi/2\,(w_{ex}^2 + w_{ox}^2/4) + (w_{ez}^2 + c^2\tau_{\mathrm{ph}}^2/4\beta^2)\,\sin^2\,\Phi/2)^{1/2}]$ (Yang *et al.*, 1999). This leads to a luminosity of $L = N_e N_{\mathrm{ph}}/[2\pi(w_{ex}^2 + w_{ox}^2/4)^{1/2}(w_{ey}^2 + w_{oy}^2/4\beta^2)^{1/2}]$ for head-on collision and, respectively, $L = N_e N_{\mathrm{ph}}/[2\pi(w_{ey}^2 + w_{oy}^2/4)^{1/2}(w_{ez}^2 + c^2\tau_{\mathrm{ph}}^2/4\beta^2)^{1/2}]$ for transverse collision. The total number of scattered X-ray photons N_γ per unit time and volume into a cone of angle θ_c is given as:

$$N_\gamma \approx 9 \times 10^7\,\frac{\text{X-ray photons}}{\text{shot}} \quad \text{for head-on collision and}$$

$$N_\gamma \approx 8 \times 10^6\,\frac{\text{X-ray photons}}{\text{shot}} \quad \text{for transverse collision,}$$

where the electron bunch was taken as focused to an spot size of $w_{ex} = 35\ \mu\mathrm{m}$, $w_{ey} = 20\ \mu\mathrm{m}$ and $w_{ez} = c\ 350$ fs. The laser was assumed to be focused to a spot size of $w_0 = 40\ \mu\mathrm{m}$ with a pulse duration of 100 fs.

In head-on geometry, the overlap integral depends only on the spot size; the laser and electron bunch durations play no role. The laser pulse travels through the electron bunch and the X-ray pulse length is determined almost entirely by the length of the electron bunch. In transverse interaction, it is noticeable from the interaction geometry (Fig. 4) that the electron bunch spot size in the x-direction w_{ex} is negligible, but the beam size in the y-direction, w_{ey} must fit with the laser spot size, and the electron bunch length w_{ez} must be comparable to the travel time of the laser pulse through the electron bunch $c\tau_{\mathrm{ph}}$. The length of the X-ray pulse will be

https://doi.org/10.1017/S0263034608000700 Published online by Cambridge University Press

dependent on how long the laser and electron beam interact. This indicates that tight electron beam focusing and short laser pulses will result in short X-ray pulses due to a minimized interaction time.The relation between these parameters and the resultant source pulse length τ_γ is expressed for head-on collision as $w_{ez}/c\beta$ and as $w_{ez}(w_{ey}^2 + c^2\tau_{ph}^2/4\beta^2 + w_{oy}^2/4)^{1/2}/[c(w_{ey}^2 + w_{ez}^2 + w_{oy}^2 + w_{oy}^2/4 + c^2\tau_{ph}^2/4\beta^2)^{1/2}]$, respectively, for transverse collision (Pogorelski *et al.*, 2000).

The T^3 laser beam transport line is shown in Figure 8. The vacuum system pumping, gauges and protection (fast valve) are designed to operate assuming no window between the laser beam transport line and the accelerator vacuum. This is necessary, as a window thick enough to withstand atmospheric let-up would be radiation-damaged by absorption of TW pulses, and a thin window will have the risk of breakage and particle contamination of ALICE in the event of a vacuum failure.

The laser beam transport line vacuum design specification is 10^{-6} mbar and the ALICE machine vacuum is at 10^{-8} mbar. The ALICE system is protected from a let-up in the laser beamline by a fast-acting valve. The laser beam propagates from the CPA compressor vessel through a concrete shielding wall, passing an optical delay line, periscoped down to the electron beam level, focused *via* an off-axis parabolic mirror (OAP) and finally turned to the interaction point. For the case of transverse interaction, the periscope is also used to rotate the polarization of the laser. The last vacuum vessel containing the OAP-mirror sits on rails allowing the focal position to be moved through the electron bunch. The focal length of the OAP-mirror is 1780 mm in head-on collision geometry and 1230 mm for transverse geometry. The scattered hard X-rays—in the direction of the electron beam—will be taken through a beryllium window to the diagnostic area (X-ray deep depletion CCD camera, fast X-ray streak camera, fast melting experiment). In head-on geometry, the last turning mirror has a hole of about 5 mm diameter to let the X-rays through and also to take a part of the laser beam out for pump-probe applications. Figure 9 shows the proposed experimental setup for the head-on collision geometry (left) and transverse collision geometry (right).

In order to model the X-ray output, it was first necessary to simulate the electron bunch spatial, angular and energy

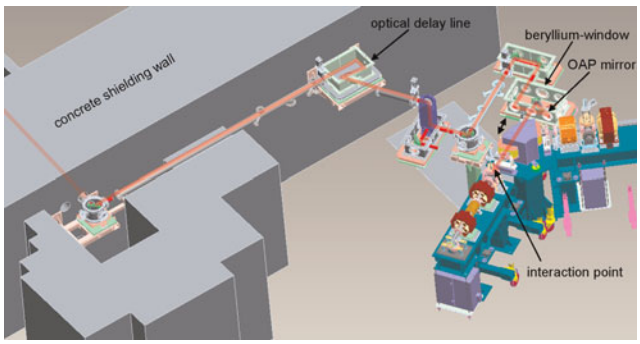

Fig. 8. (Color online) Laser beam transport line through the concrete shielding wall to the interaction region.

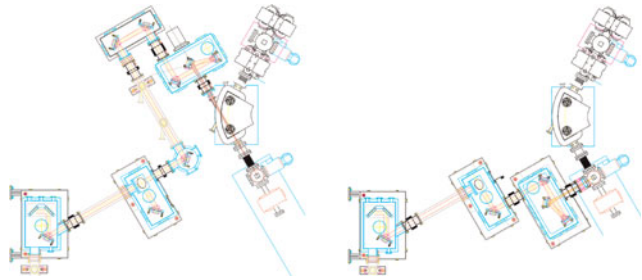

Fig. 9. (Color online) Experimental setup for head-on collision (left) and transverse collision (right).

distribution at the interaction point. For optimal generation of Compton scattered X-rays, the ALICE lattice is set to focus the electrons to give the highest electron density at the interaction point. This maximizes the X-ray flux and also reduces the size of the X-ray source. The electron trajectories were modeled using the particle tracking code ELEGANT. In excess of 100,000 electrons were tracked through to the focus. The electron distribution produced was then used as input to code written to simulate the inverse Compton scattering. The electron data consisted of the electron position at the focus plane, the electron direction vector (direction cosines), and the electron energy. The laser photons were taken as a Gaussian angular distribution (in the horizontal and the vertical planes) and an energy distribution given by the transform function of the laser Gaussian temporal distribution. For each electron at the focus, a laser photon was generated at random by the code with direction vector and energy randomly chosen according to their assumed distributions. An X-ray was then generated with direction vector selected randomly conforming to the Klein-Nishina cross-section. The calculated X-ray energy as a function of emission angle in head-on scattering geometry is shown in Figure 10 and for transverse scattering

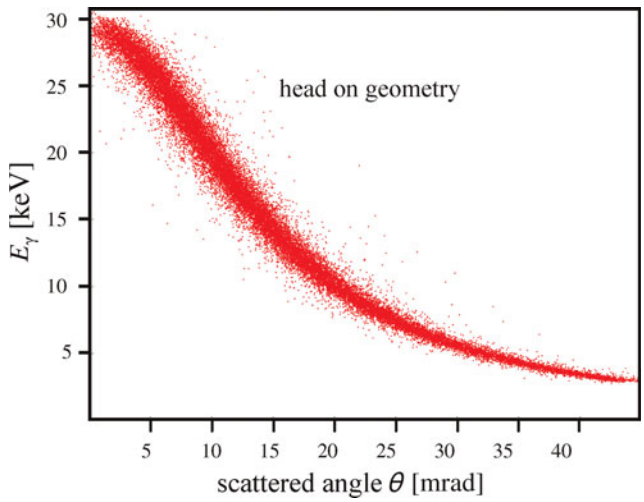

Fig. 10. (Color online) X-ray energy E_γ versus the emission angle θ in head-on scattering geometry.

https://doi.org/10.1017/S0263034608000700 Published online by Cambridge University Press

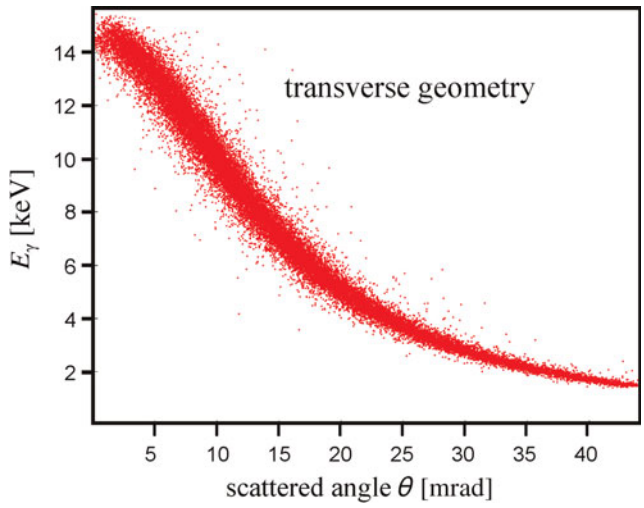

Fig. 11. (Color online) X-ray energy E_γ as a function of the emission angle θ in side scattering geometry.

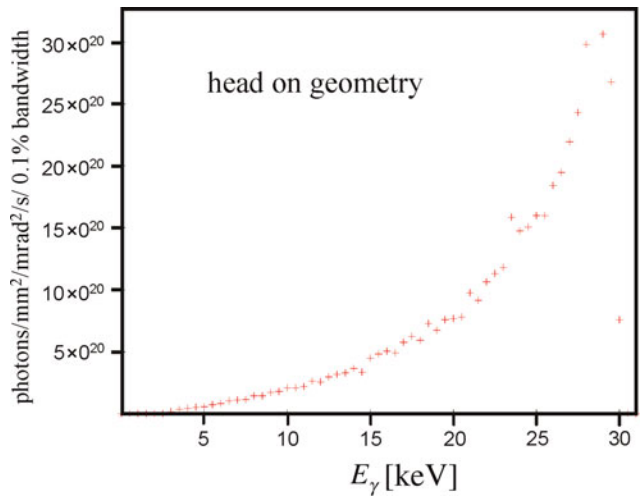

Fig. 12. (Color online) Spectral brightness of the X-ray source versus E_γ for head-on scattering geometry.

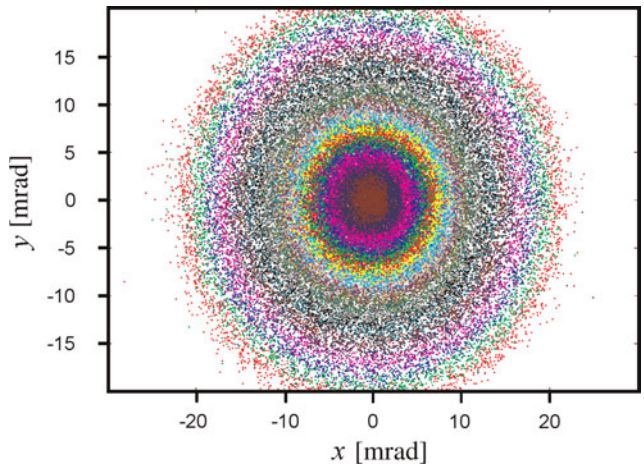

Fig. 13. (Color online) Angular distribution of the X-rays generated in head-on collision geometry; each colour is a 1 keV energy band with 20–21 keV on outside and 30–31 keV at the centre.

geometry in Figure 11, respectively. The spectral brightness of the X-ray source (photons/(mm^2 mrad^2 s 0.1% bandwidth) is shown in Figure 12. Figure 13 shows the angular distribution of the X-rays for head-on geometry.

CONCLUSION AND OUTLOOK

COBALD is an instrument capable of generating high peak brightness fs X-ray pulses. X-rays generated by the interaction of the table-top multi-10 TW laser with electron bunches have been modeled by Monte Carlo simulation calculating over 10^5 interactions, and have shown that a brightness in excess of 10^{21} X-rays/(mm^2 mrad^2 s 0.1% bandwidth) will be obtained in head-on geometry. It is intended to operate COBALD in both counter-propagating and transverse interaction geometry. The peak X-ray energy is about 30 keV in head-on geometry and approximately 15 keV in transverse scattering geometry. The X-ray pulse length in head-on mode will be about 350 fs and in transverse scattering geometry about 100 fs. The X-ray source size will be of order 20×35 μm^2. Characterization of the X-ray beam profile and energy spectrum will provide vital information about the spatial and temporal structure of the electron beam in the ALICE. Further studies are planned to examine photon/electron beam synchronization and source stability; this is a necessary requirement prior to any dynamic experiments being performed. The availability of this ultra-short brilliant X-ray source will allow X-ray diffraction and spectroscopy techniques to be extended into the time domain allowing atomic resolution probing of structural dynamics. This type of experiment could be carried out using a pump pulse—for example, by extracting a fraction of the multi-10 TW laser pulse—to start a time-dependent process in a sample. The sample could then be probed, after a short delay, by the X-ray pulse. This would allow, for example, intermediate species to be probed during chemical reactions or strain relaxation following lattice distortion to be measured.

ACKNOWLEDGEMENT

We would like to acknowledge the financial support of STFC and the Northwest Development Agency, through the Northwest Science Fund.

REFERENCES

Abdallah, J., Batani, D., Desai, T., Lucchini, G., Faenov, A., Pikuz, T., Magunov, A. & Narayanan, V. (2007). High resolution X-ray emission spectra from picosecond laser irradiated Ge targets. *Laser Part. Beams* **25**, 245–252.

Alferov, D.F., Bashmakov, Yu. & Bessonov, E.G. (1974). Undulator radiation. *Sov. Phys. Tech. Phys.* **18**, 1337.

Arthur, G., Materlik, A.G., Tatchyn, R. & Winick, H. (1995). The LCLS: A fourth generation light source using the SLAC linac. *Rev. Sci. Instr.* **66**, 1987.

https://doi.org/10.1017/S0263034608000700 Published online by Cambridge University Press

Baeva, T., Gordienko, S. & Pukhov, A. (2007). Relativistic plasma control for single attosecond pulse generation: Theory, simulations, and structure of the pulse. *Laser Part. Beams* **25**, 339–346.

Baker, S., Robinson, J.S., Haworth, C.A., Teng, H., Smith, R.A., Chiril, C.C., Lein, M., Tisch, J.W. & Marangos, J.P. (2006). Probing proton dynamics in molecules on an attosecond timescale. *Science* **312**, 4247.

Bazerov, I., Belomestnykh, S., Bilderback, D., Finkelstein, K., Fontes, E., Gray, S., Gruner, S.M., Krafft, G.A., Merminga, H., Helmke, R., Rogers, J., Sinclair, C., Talman, R. & Tigner, M. (2001). Study for a proposed phase I energy recovery linac (ERL) synchrotron light source. CHESS Technical Memo 01-003, JLAB-ACT-01-04. Ithica: Cornell University.

Berden, G., Jamison, S.P., MacLeod, A.M., Gillespie, W.A., Redlich, B. & van der Meer, A.F.G. (2004). Electro-optic technique with improved time resolution for real-time, nondestructive, single-shot measurements of femtosecond electron bunch profiles. *Phys. Rev. Lett*. **93**, 114802.

Borland, M. (2006). Evaluation of the possibility of upgrading the advanced photon source to an energy recovery linac. *Nucl. Instr. Meth. A* **557**, 224–229.

Brabec, T., Spielmann, Ch., Curley, P.F. & Krausz, F. (1992). Kerr lens mode locking. *Opt. Lett*. **17**, 1292.

Brown, L.S. & Kibble, T.W.B. (1964). Interaction of intense laser beams with electrons. *Phys. Rev*. **133**, A705.

Catravas, P., Esarey, E. & Leemans, W.P. (2001). Femtosecond Thomson scattering X-ray source based on laser wakefield accelerator for ultrafast X-ray absorption spectroscopy. *Meas. Sci. Technol*. **12**, 1828.

Chen, L.M., Kando, M., Xu, M.H., Li, Y.T., Koga, J., Chen, M., Xu, H., Yuan, X.H., Dong, Q.L., Sheng, Z.M., Bulanov, S.V., Kato, Y., Zhang, J. & Tajima, T. (2008). Study of X-ray emission: Enhancement via a high-contrast femtosecond laser interacting with a solid foil. *Phys. Rev. Lett*. **100**, 045004.

Chouffani, K., Harmon, F., Wells, D., Jones, J. & Lancaster, G. (2006). Laser-Compton scattering as a tool for electron beam diagnostics. *Laser Part. Beams* **24**, 411.

Coisson, R. (1979). Angular-spectral distribution and polarization of synchrotron radiation from a "short" magnet. *Phys. Rev. A* **20**, 524.

Compton, A.H. (1923). A quantum theory of the scattering of X-rays by light elements. *Phys. Rev*. **21**, 207 & 483.

Divall, E.J. & Ross, I.N. (2004). High dynamic range contrast measurements by use of an optical parametric amplifier correlator. *Opt. Lett*. **29**, 2273.

Giulietti, D., Galimberti, M., Giulietti, A., Gizzi, L.A., Labate, L. & Tomassini, P. (2005). The laser-matter interaction meets the high energy physics: Laser-plasma accelerators and bright gamma X-ray sources. *Laser Part. Beams* **23**, 309.

Gruner, S.M. & Tigner, M. (2001). Study for a proposed phase I energy recovery linac (ERL) synchrotron light source. CHESS Technical Memo 01-003, JLAB-ACT-01-04. Ithica: Cornell University.

Guo, T., Spielmann, C., Walker, B.C. & Barty, C.P.J. (2001). Generation of hard X-rays by ultrafast terawatt lasers. *Rev. Sci. Instrum*. **72**, 41.

Hafz, N., Lee, H.J., Kim, G.H., Suk, H. & Lee, J. (2003). Femtosecond X-ray generation via the Thomson scattering of a terawatt laser from electron bunches produced from the LWFA utilizing a plasma density transition. *IEEE Trans. Plasma Sci*. **31**, 1388.

Hartemann, F.V., Baldis, H.A., Kerman, A.K., Le Foll, A., Luhmann, N.C. & Rupp, B. (2001). Three-dimensional theory of emittance in Compton scattering and X-ray protein crystallography. *Phys. Rev. E* **64**, 016501.

Hartemann, F.V., Brown, W.J., Gibson, D.J., Anderson, S.G., Tremaine, A.M., Springer, P.T., Wootton, A.J., Hartouni, E.P. & Barty, C.P.J. (2005). High-energy scaling of Compton scattering light sources. *Phys. Rev. Spec. Top*. **8**, 100702.

Hartemann, F.V., Tremaine, A.M., Anderson, S.G., Barty, C.P.J., Betts, S.M., Booth, R., Brown, W.J., Crane, J.K., Cross, R.R., Gibson, D.J., Fittinghoff, D.N., Kuba, J., Le Sage, G.P., Slaughter, D.R., Wootton, A.J., Hartouni, E.P., Springer, P.T., Rosenzweig, J.B. & Kerman, A.K. (2004). Characterization of a bright tunable ultrafast Compton scattering X-ray source. *Laser Part. Beams* **22**, 221–244.

Helliwell, J.R. & Rentzepis, P.M. (1997). Time-resolved diffraction. In *Time-Resolved X-ray and Electron Diffraction*. Oxford: Oxford University Press.

Jamison, S.P., MacLeod, A.M., Berden, G., Jaroszynski, D.A. & Gillespie, W.A. (2006). Temporally resolved electro-optic effect. *Opt. Lett*. **31**, 1753.

Jamison, S.P., Shen, J., MacLeod, A.M., Gillespie, W.A. & Jaroszynski, D.A. (2003). High-temporal-resolution, single-shot characterization of terahertz pulses. *Opt. Lett*. **28**, 1710.

Janulewicz, K.A., Lucianetti, A., Priebe, G. & Nickles, P.V. (2004*a*). Review of state-of-the-art and output characteristics of table-top soft X-ray lasers. *X-ray Spec*. **33**, 262–266.

Janulewicz, K.A., Priebe, G., Tümmler, J. & Nickles, P.V. (2004*b*). Single-pulse low-energy-driven transient inversion X-ray lasers. *IEEE J. Quant. Electr*. **10**, 1368–1372.

Janulewicz, K.A., Tummler, J., Priebe, G. & Nickles, P.V. (2005). Plasmakinetics perspective of a collisional Ni-like X-ray laser pumped by a single profilled laser pulse. *Phys. Rev. A* **72**, 043825.

Khattak, F., Saiz, E.G., Dzelzainis, T., Riley, D. & Zhai, Z. (2007). Scale-length optimizing of short pulse Cu K-alpha laser plasma sources. *Appl. Phys. Lett*. **90**, 081502.

Kim, K.J. (1989). Physics of particle accelerators. *AIP Conf. Proc*. **184**, 565.

Kim, K.J., Chattopadhyay, S. & Shank, C.V. (1994). Generation of femtosecond X-rays by 90 degrees Thomson scattering. *Nucl. Instr. Meth. A* **341**, 351.

Klein, O. & Nishina, Y. (1929). Über die Streuung von Strahlung durch freie Elektronen nach der neuen relativistischen Quantendynamik von Dirac (About the scattering of radiation by free electrons after the new relativistic quantum dynamics of Dirac). *Zeit. f. Phys*. **52**, 853.

Krafft, G.A. (2004). Spectral distributions of Thomson-scattered photons from high-intensity pulsed lasers. *Phys. Rev. Lett.* **92**, 204802.

Krafft, G.A., Doyuran, A. & Rosenzweig, J.B. (2005). Pulsed-laser nonlinear Thomson scattering for general scattering geometries. *Phys. Rev. E* **72**, 056502.

Kulipanov, G.N., Skrinsky, A.N. & Vinokurov, N.A. (1998). Synchrotron light sources and recent developments of accelerator technology. *J. Sync. Radiat*. **5**, 176.

Landau, L.D. & Lifshitz, E.M. (1975). *Classical Theory of Fields. Butterworth-Heinemann*. Oxford: Oxford University Press.

Leemans, W., Chattopadhyay, S., Esarey, E., Zholents, A., Zolotorev, M., Chin, A., Schoenlein, R. & Shank, C. (2000).

Femtosecond X-ray generation through relativistic electron beam-laser interaction. *Phys. Astrophys*. **1**, 279–296.

Leemans, W.P., Schoenlein, R.W., Volfbeyn, P., Chin, A.H., Glover, T.E., Balling, P., Zolotorev, M., Kim, K.-J., Chattopadhyay, S. & Shank, C.V. (1997). Interaction of relativistic electrons with ultrashort laser pulses: generation of femtosecond X-rays and microprobing of electron beams. *IEEE J. Quan. Electron*. **33**, 1925–1934.

Leemans, W.P., Volfbeyn, P., Zolotorev, M., Kim, K.J., Chattopadhyay, S., Schoenlein, R., Balling, P., Shank, C.V., Chin, A. & Glover, E. (1996). Laser-based sub-picosecond electron bunch characterization using 90 degrees Thomson scattering. *Phys. Rev. Lett*. **77**, 4182.

Legall, H., Stiel, H., Arkadiev, V. & Bjeoumikhov, A.A. (2006). High spectral resolution X-ray optics with highly oriented pyrolytic graphite. *Opt. Express* **14**, 10.

Li, Y., Huang, Z., Borland, M.D. & Milton, S. (2002). Small-angle Thomson scattering of ultrafast laser pulses for bright, sub-100-fs X-ray radiation. *Phys. Rev*. **5**, 044701.

Lucianetti, A., Janulewicz, K.A., Kroemer, R., Priebe, G., Tummler, J., Sandner, W., Nickles, P.V. & Redkorechev, V.I. (2004). Transverse spatial coherence of a transient nickellike silver soft-X-ray laser pumped by a single picosecond laser pulse. *Opt. Lett*. **29** (8), 881–883.

Mangles, S.P.D., Walton, B.R., Najmudin, Z., Dangor, A.E., Krushelnick, K., Malka, V., Manclossi, M., Lopes, N., Carias, C., Mendes, G. & Dorchies, F. (2006). Table-top laser-plasma acceleration as an electron radiography source. *Laser Part. Beams* **24**, 185–190.

Materlik, A.G., Tatchyn, R. & Winick, H. (1995). The LCLS: A fourth generation light source using the SLAC linac. *Rev. Sci. Instr*. **66**, 1987.

Neil, G.R., Behre, C., Benson, S.V., Bevins, M., Biallas, G., Boyce, J., Coleman, J., Dillon-Townes, L.A., Douglas, D., Dylla, H.F., Evans, R., Grippo, A., Gruber, D., Gubeli, J., Hardy, D., Hernandez-Garcia, C., Jordan, K., Kelley, M.J., Merminga, L., Mammosser, J., Moore, W., Nishimori, N., Pozdeyev, E., Preble, J., Rimmer, R., Shinn, M., Siggins, T., Tennant, C., Walker, R., Williams, G.P. & Zhang, S. (2005). *The JLab High Power ERL Light Source, The 32nd Advanced ICFA Beam Dynamics Workshop on Energy Recovering Linacs*. Newport News, VA: Jefferson Lab.

Notley, M.M., Weber, R.L., Fell, B., Jeffries, J., Freeman, R.R., Mackinnon, A.J., Dickson, R., Hey, D., Khattak, F., Saiz, E.G. & Gregori, G. (2006). Development of time resolved X-ray spectroscopy in high intensity laser-plasma interactions. *Rev. Sci. Instr*. **77**, 10F322.

Ozaki, T., Kieffer, J.C., Toth, R., Fourmaux, S. & Bandulet, H. (2006). Experimental prospects at the Canadian advanced laser light source facility. *Laser Part. Beams* **24**, 101–6.

Phuoc, K.Ta., Rousse, A., Pittman, M., Rousseau, J.P., Malka, V., Fritzler, S., Umstadter, D. & Hulin, D. (2003). X-Ray radiation from nonlinear Thomson scattering of an intense femtosecond laser on relativistic electrons in a helium plasma. *Phys. Rev. Lett*. **91**, 195001.

Pogorelski, I.V., Ben-Zvi, I., Hirose, T., Kashiwagi, S., Yakimenko, V., Kusche, K., Siddons, P., Skaritka, J., Kumita, T., Tsunemi, A., Omori, T., Urakawa, J., Washio, M., Yokoya, K., Okugi, T., Liu, Y., He, P. & Cline, D. (2000). Demonstration of 8×10^{18} photons/second peaked at 1.8 Å in a relativistic Thomson scattering experiment. *Phys. Rev*. **3**, 090702.

Poole, M.W., Bennett, S.L., Bowler, M.A., Bliss, N., Dykes, D.M., Farrow, R.C., Gerth, C., Holder, D.J., MacDonald, M.A., Muratori, B., Owen, H.L., Quinn, F.M., Seddon, E.A., Smith, S.L., Suller, V.P., McNeil, B.J., Ross, I.N. & Thompson, N.R. (2003). 4GLS: A new type of fourth generation light source facility. *Proc. of the 2003 Particle Accelerator Conference*, pp. 189–191. Piscataway, NJ: IEEE.

Priebe, G., Redkorechev, V.I., Janulewicz, K.A. & Nickles, P.V. (2006). Pulse shape measurement by a non-collinear third-order correlation technique. *Opt. Commun*. **259**, 848.

Ride, S.K., Esarey, E. & Baine, M. (1995). Thomson scattering of intense lasers from electron beams at arbitrary interaction angles. *Phys. Rev. E* **52**, 5425.

Riley, D., Angulo-Gareta, J.J., Khattak, F.Y., Lamb, M.J., Foster, P.S., Divall, E.J., Hooker, C.J., Langley, A.J., Clarke, R.J. & Neely, D. (2005). Kα yields from Ti foils irradiated with ultrashort laser pulses. *Phys. Rev. E* **71**, 016406.

Ross, M.C., Alley, R., Arnett, D., Bong, E., Colocho, W., Frisch, J., Hortonsmith, S., Inman, W., Jobe, K., Kotseroglou, T., McCormick, D., Nelson, J., Scheeff, M. & Wagner, S. (1997). A laser-based beam profile monitor for the SLC/SLD interaction region. *AIP Conf. Proc.* **390**, 281–289.

Salamin, Y.I. & Faisal, F.H.M. (1996). Harmonic generation by superintense light scattering from relativistic electrons. *Phys. Rev. A* **54**, 4383.

Sansone, G., Benedetti, E., Calegari, F., Vozzi, C., Avaldi, L., Flammini, R., Poletto, L., Villoresi, P., Altucci, C., Velotta, R., Stagira, S., De Silvestri, S. & Nisoli, M. (2006). Isolated single-cycle attosecond pulses. *Science* **314**, 443.

Sarachik, E.S. & Schappert, G.T. (1970). Classical theory of the scattering of intense laser radiation by free electrons. *Phys. Rev. D* **1**, 2738.

Schoenlein, R.W., Chattopadhyay, S., Chong, H.H.W., Glover, T.E., Heimann, P.A., Shank, C.V., Zholents, A.A. & Zolotorev, M.S. (2000*a*). Generation of femtosecond pulses of synchrotron radiation. *Science* 2237.

Schoenlein, R.W., Chattopadhyay, S., Chong, H.H.W., Glover, T.E., Heimann, P.A., Leemans, W.P., Shank, C.V., Zholents, A. & Zolotorev, M. (2000*b*). Generation of femtosecond X-ray pulses via laser-electron beam interaction. *Appl. Phys. B* **71**, 1–10.

Schoenlein, R.W., Leemans, W.P., Chin, A.H., Volfbeyn, P., Glover, T.E., Balling, P., Zolotorev, M., Kim, K.J., Chattopadhyay, S. & Shank, C.V. (1996). Femtosecond X-ray pulses at 0.4 Å generated by 90° Thomson scattering: A tool for probing the structural dynamics of materials. *Science* **274**, 236.

Service, R.F. (2002). Battle to become the next generation X-ray source. *Science* **298**, 1356.

Siders, W., Cavalleri, A., Sokolowski-Tinten, K., Tóth, Cs., Guo, T., Kammler, M., Wilson, K.R., von der Linde, D. & Barty, C.P.J. (1999). Detection of nonthermal melting by ultrafast X-ray diffraction. *Science* **286**, 1340.

Smith, S.L., Muratori, B.D., Owen, H.L., Hoffstaetter, G.H., Litvinenko, V.N., Ben-Zvi, I., Bai, M., Beebe-Wang, J., Blaskiewicz, M., Calaga, R., Fischer, W., Chang, X.Y., Kayran, D., Kewisch, J., MacKay, W.W., Montag, C., Parker, B., Ptitsyn, V., Roser, T., Ruggiero, A., Satogata, T., Surrow, B., Tepikian, S., Trbojevic, D., Yakimenko, V., Zhang, S.Y. & Piot, P. (2005). Optics designs of ongoing ERL projects. *Nucl. Instr. Meth. A* **557**, 145–164.

Smith, S.L., Bliss, N., Goulden, A.R., Holder, D.J., McIntosh, P.A. & Priebe, G. (2007). The status of the Daresbury energy recovery linac prototype. *IEEE Part. Acc. Conf.* **1–11**, 3305–3307.

Sokolowski-Tinten, K. & von der Linde, D. (2004). Ultrafast phase transitions and lattice dynamics probed using laser-produced X-ray pulses *J. Phys. Condens. Matter* **16**, R1517–R1536.

Spence, D.E., Kean, P.N. & Sibbett, W. (1991). 60-fsec pulse generation from a self-mode-locked Ti:sapphire laser. *Opt. Lett*. **16**, 42.

Stingl, A., Lenzner, M., Spielmann, Ch., Krausz, F. & Szipocs, R. (1995). Sub-10-fs mirror-dispersion-controlled Ti:sapphire laser. *Opt. Lett*. **20**, 602.

Strickland, D. & Mourou, G. (1985). Compression of amplified chirped optical pulses. *Opt. Com*. **56**, 219.

Sundaram, S.K. & Mazur, E. (2002). Inducing and probing non-thermal transitions in semiconductors using femtosecond laser pulses. *Nat. Mat.* **1**, 217–224.

Suwada, T., Iida, N., Funakoshi, Y., Kawamoto, T. & Kikuchi, M. (1997). First beam test result of a prototype wire scanner for the KEKB injector linac and BT lines. *Proc. of 11th Symp. Acc. Tech. Sc., Ako, Hyogo, Japan*, 97–184.

Tannebaum, P. & Shintake, T. (1999). Measurement of small electron-beam spots. *Ann. Rev. Nucl. Part. Sci*. **49**, 125–162.

Tigner, M. (1965). A possible apparatus for electron clashing experiments. *Nuovo Cimento* **37**, 1228–1231.

Tomov, I.V., Oulianov, D.A., Chen, P. & Rentzepis, P.M. (1999). Ultrafast time-resolved transient structures of solids and liquids studied by means of X-ray diffraction and EXAFS. *J. Phys. Chem. B*. **103**, 7081.

Tümmler, J., Janulewicz, K.A., Priebe, G. & Nickles, P.V. (2005). 10-Hz grazing-incidence pumped Ni-like Mo X-ray laser. *Phys. Rev. E* **72**, 037401.

Umstadter, D. (2003). Relativistic laser plasma interactions. *J. Phys. D: Appl. Phys*. **36**, R151.

von der Linde, D. (2003). A picosecond view of melting. *Science* **302**, 1345.

von Laue, M. (1936). Die äußere form der kristalle in ihrem einfluß auf die interferenzerscheinungen an raumgittern. *Annalen der Physik* **26**, 55.

Wark, J. (1999). X-ray diffraction: Table-top picosecond sources. *Nature* **398**, 284–285.

Watson, J.D. & Crick, F.H.C. (1953). Implications of the structure of deoxyribonucleic acid. *Nature* **171**, 964–967.

Xia, B., Li, Z., Kang, K., Huang, W., Huang, G., He, X., Du, Y. & Tang, C. (2004). Evaluation and simulations of a Thomson scattering X-ray source based on ray tracing methods. *Laser Part. Beams* **22**, 355.

Yang, J., Washio, M., Endo, A. & Hori, T. (1999). Evaluation of fs X-rays produced by Thomson scattering under linear and non-linear interactions between a low-emittance electron beam and an intense polarized laser light. *Nucl. Instr. Meth. Phys. Res. A* **428**, 556.

Zhavoronkov, N., Gritsai, Y., Bargheer, M., Woerner, M. & Elsaesser, T. (2005). Generation of ultrashort Kα radiation from quasipoint interaction area of femtosecond pulses with thin foils. *Appl. Phys. Lett*. **86**, 244107.

https://doi.org/10.1017/S0263034608000700 Published online by Cambridge University Press